In-line monitoring of the freeze-drying process by means of heat flux sensors

In-line monitoring of freeze-drying processes by means of heat flux sensors

Camilla Moino[‡,§], Erwan Bourlès[‡], Roberto Pisano[§], Bernadette Scutellà[*,‡]

[‡] GSK Vaccines, 89 Rue de l'Institut, 1330 Rixensart, Belgium

[§] Department of Applied Science and Technology, 24 Politecnico di Torino, corso Duca degli Abruzzi, 10129 Torino, Italy

[*]*E-mail of the corresponding author:* bernadette.z.scutella@gsk.com

ABSTRACT

The final qualities of a pharmaceutical product can be adversely affected by a sub-optimized freeze-drying process. Multiple variables and operating conditions come into play, thus making the overall process difficult to control. In this study, we show how heat flux sensors can guide the in-line monitoring of freezing and primary drying of placebo formulations, leading to significant insights that contribute to our understanding of the phenomena involved. It was found that heat flux sensors can be used as a practical and robust tool to monitor a lyophilization cycle, by defining processing time and investigating different process scenarios. Concerning the freezing step, the heat flux sensors proved to be an effective way to detect both the nucleation and end of crystal growth. Additionally, the sensors' signal highlighted the end of cooling and freezing steps and thus helped to eliminate uncertainty about the time required to reach thermal equilibrium across the batch. An ultimate potential of the devices was addressed to build the design space for freezing and primary drying, laying the foundations for new research in this topic.

1 INTRODUCTION

Freeze-drying is widely used to process heat-sensitive products with the aim to increase their shelf life. The quality of the final product strictly depends on the microstructure formed during freezing and thus careful control of the freezing step is of upmost importance for the success of the overall process.[1,2] Freezing involves two main phenomena, which are ice nucleation and ice crystal growth. During nucleation, water molecules gather

into clusters, resulting in stable ice crystals at the nanometric scale. Supercooling is defined as the retention of the liquid state below the equilibrium freezing point of the solution. A higher degree of supercooling grants the formation of smaller ice crystals, resulting in a higher product resistance to vapor flow, hence a lower primary drying rate.[1–6] Nucleation occurs stochastically, especially with deeper subcooling and in the presence of contaminants, additives, or any other structure or impurity that can serve as an ice nucleating agent. In such random conditions, vials across the batch can nucleate at different times and different temperatures. This variation leads to product heterogeneity, which makes the vials behave differently during primary drying. Vial-to-vial heterogeneity can result in excessively long runs to accommodate the slowest-drying vials, with an increase in manufacturing costs and a reduced plant capacity as consequences.[3] Therefore, various controlled nucleation technologies have been put forward to eliminate or mitigate any heterogeneity in nucleation temperature. In this study, we used the ice-fog technique to instantaneously initiate the nucleation event; the key principle of this method relies on the creation of ice crystals that are forced into the vials and act as nucleation seeds.[1,2] Such a technology induces the nucleation event in all the vials of the batch within a narrow range of temperature and time[7] and, thus, directly controls product morphology.

The heterogeneity of heat transfer during primary drying is also a potential issue. Here, atypical heat transfer can occur as a result of different positions in the batch, leading to differences in sublimation rates.[8–10]

It is therefore necessary to control the process through the monitoring of its key variables and many tools have been developed to this purpose.[11,12] Product temperature can be monitored by means of miniature thermocouples or resistance temperature detectors, which allow the collection of reliable data throughout the process. Pressure in the chamber can be measured by pressure transducers, such as thermal conductivity-type sensors and capacitance manometers. Moreover, the use of comparative pressure measurement is widely adopted as a process-monitoring tool to define the end point of both primary and secondary drying.[13,14] Recent works have shown similar potential for mass spectroscopy, which might be used to end the cycle at a precise residual moisture level.[14,15] Finally, the heat flux exchanged in discrete locations throughout the process can be monitored by heat flux sensors. These are thin-film differential thermopiles that can convert the temperature difference across them into a voltage value as a result of the Seebeck effect and then convert it into the proportional heat flux.[16] Heat flux sensors have many interesting potentials,[12] one of these being the ability to measure thermal events during freezing. Secondly, they allow the measurement of the product temperature during primary drying without the need for a thermocouple as long as the vial thermal conductivity is known. In addition, these useful applications do not impede heat flow.

In this study, we investigated the suitability of heat flux sensors for the in-line monitoring of a freeze-drying process. We highlighted useful features during both freezing and primary drying.

2 MATERIALS AND METHODS

2.1 Materials

The experiments were performed by using 15% (w/w) sucrose (VWR BDH Chemicals, Leuven, Belgium) in water for injection. Filling the vials was accomplished by a dedicated machine (ROTA, Gif-sur-Yvette, France). In particular, one mL of sucrose solution was poured in 3 mL siliconized tubing vials (Müller + Müller, Holzminden, Germany) and partially closed with igloo stoppers (FM 460 type, Helvoet, Lommel, Belgium).

2.2 Instrument and Equipment

All cycles were carried out in a pilot-scale freeze-dryer (REVO, Millrock, Kingston, NY, USA) equipped with four temperature-controlled shelves numbered from the top to the bottom, each offering a shelf area of 0.186 m^2. A refrigeration system was necessary to achieve low temperatures; it consisted of four components: a compressor, a condenser, an expansion device, and an evaporator. When needed, a second refrigeration loop could be put in a series with the first one. The condenser also served for the extraction of condensable products and was connected to the drying chamber by means of a butterfly valve. Both a capacitance manometer (Manometer, MKS Instruments, Munich, Germany) and a thermal conductivity gauge (Pirani, MKS Instruments, Munich, Germany) were used to monitor the pressure inside the chamber.

The freeze-dryer was equipped with three heat flux sensors (AccuFlux, Millrock, Kingston, KY, USA).

A FreezeBooster Control Nucleation Station (Millrock, Kingston, NY, USA) was used to trigger the nucleation event exploiting the ice-fog technique; in particular, ice crystals were injected into the product chamber under chosen conditions, i.e., injected water volume and nucleation temperature. The desired volume of injected water could be set in the range 10–50 mL according to batch size and filling volume; unless otherwise stated, 20 mL was chosen.

The product temperature throughout the overall cycle was measured by means of T-type thermocouples (Pharmatech, Terni, Italy),[12] which were placed at the bottom of selected vials. The end of freezing was determined with the heat flux sensors while the primary drying endpoint was revealed by comparative pressure measurement.[13,14]

2.3 Process monitoring via heat flux sensors

2.3.1 Experimental set up

The heat flux exchanged between the shelves and the vials was monitored by three heat flux sensors (AccuFlux, Millrock, Kingston, NY, USA). These heat flux sensors were mounted at the centre of the second shelf and on the second and third shelves, near the external door. The detection area was 59 mm $\times$ 56.5 mm. Figure 1 represents a scheme of the sensor arrangement on the second shelf while Figure 2 shows a view of the edge sensor on the second shelf, above which some vials are positioned.

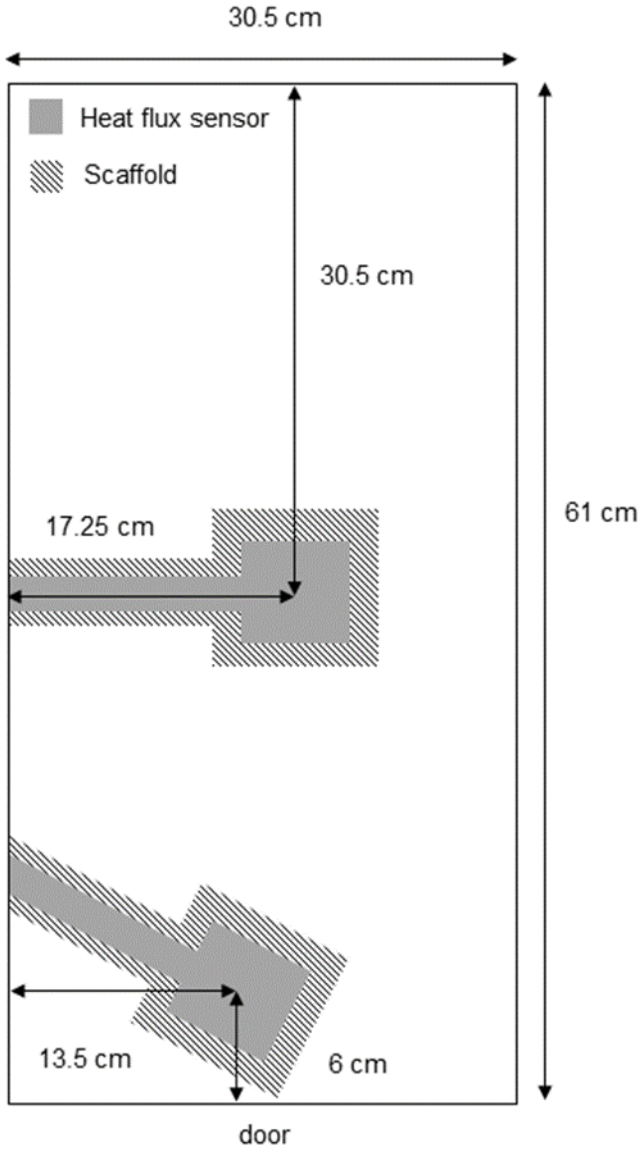

Figure 1. Schematic drawing of the freeze-dryer second shelf, where two heat flux sensors (in central and edge positions) are mounted (drawing to scale).

Figure 2. View of the edge sensor on the second shelf of the freeze-dryer.

In all the tests performed, heat flow was > 0 when the heat flowed from the shelf toward the set of vials and vice versa. Furthermore, bottomless trays of different sizes (140 or 753 vials) were used to facilitate the loading/unloading of vials from the freeze-dryer. The vials were arranged in hexagonal clusters and the maximum number of vials per sensor was:

$$N_v = \frac{a \times b \times \frac{\pi\sqrt{3}}{6}}{\pi r^2} \quad (1)$$

where a and b are the sensor sizes and r is the vial radius equal to 8.12×10^{-3} m.

2.3.2 Design of experiments

Seven experiments were carried out in total, the details of which are summarized in Table 1. We used two different batch configurations: three trays of 140 vials each, positioned on the shelves covering each sensor and equipped with two thermocouples each (partial loading); two trays of 753 vials each, positioned onto the second and third shelves and supplied with four thermocouples each, two at the center and two on the edge of every shelf (mid loading). For each test, the temperature profiles measured by thermocouples located in the same portion of the batch were compared and were in any case found to be quite similar, indicating that the value should be reliable.

Table 1. Freezing details of the performed cycles

Cycle	Batch loading	Cooling	Holding		Controlled nucleation	Post-nucleation freezing method
			T_n, °C	t, min		
CN1	partial	- 1 °C/min	- 6	30	Yes	- 1 °C/min
CN2	partial	*	- 6	*	Yes	*
PD1	mid	- 1 °C/min	- 6	30	Yes	- 1 °C/min
MCN1	partial	- 1 °C/min	- 6	30	Yes	- 1 °C/min
MSN1	partial	- 1 °C/min	–	–	No	- 1 °C/min
MPD1	mid	- 1 °C/min	- 6	30	Yes	- 1 °C/min
MPD2	mid	- 1 °C/min	–	–	No	- 1 °C/min

* chosen by the equipment while using the LyoPAT feature

Different cycles were run, called CN1, CN2, PD1, MCN1, MSN1, MPD1 and MPD2. For the sake of clarity, the acronyms were chosen to highlight the step on which the investigation was focused. Thus, CN stands for controlled nucleation, SN for spontaneous nucleation, and PD for primary drying. Moreover, if the name of the cycle begins with the letter M, this indicates that the objective of the test was to focus on the in-line monitoring of the cycle. Made these assumptions, CN1, CN2 and PD1 aimed to validate the AccuFlux sensor's signal while MCN1, MSN1, MPD1 and MPD2 were conducted for the in-line monitoring of freezing and primary drying. CN1, CN2, MCN1 refer to freezing cycles run with controlled nucleation. PD1 and MPD1 refer to complete freeze-drying cycles run with controlled nucleation while MPD2 to a freeze-drying cycle run with spontaneous nucleation. Primary drying in the three latter tests was carried out at – 27 °C and 0.1 mbar following a 0.5-hour ramp once the freezing step was finished in order to reach the desired conditions. MSN1 refers to a freezing cycle run with spontaneous nucleation. CN1, PD1 and MCN1 were repeated twice to test the repeatability of the sensors' outcomes.

2.3.3 Validation of the heat flux sensor's signal

As a starting point, the signal of the heat flux sensor was calibrated by comparison with the theoretical value calculated for the initial cooling step when the liquid was cooled down to the nucleation temperature. Such a comparison was carried out for partial load conditions, focusing on the central AccuFlux sensor (see CN1 in Table 1).

Based on the product temperature signal, the evolution of the sensible heat per unit of time can be calculated as follows:

$$\dot{Q_{c,\iota}} = m_{s,i} Cp_{s,i} \frac{(T_i - T_{i-1})}{\Delta t} \quad (2)$$

where Δt is the time step for the data collection and was equal to 60 s. Specific heat capacity varies with temperature as described in Table 2. The resulting $\dot{Q_{c,\iota}}$ corresponds to the sensible heat exchanged by the sensor; thus, it was divided by the sensor size to obtain $J_{q,i}$, which was finally compared with the heat flux recorded by the corresponding sensor.

Table 2. Physical properties and operative conditions used in this study

Symbol	Description	Value	Units	Reference
ΔH_c	Solution [a] enthalpy of crystallization	- 235	kJ kg^{-1}	[35]
ΔH_s	Enthalpy of sublimation of water	2839	kJ kg^{-1}	[36]

ρ_s	Solution [a] mass density [b]	1.059	kg dm^{-3}	18,19
ρ_f	Frozen [a] mass density [c]	0.982	kg dm^{-3}	17,18
T_n	Nucleation temperature	- 6	°C	
T_f	Freezing temperature	- 56	°C	
$Cp_s(T)$	Solution [a] specific heat [b d]	$0.00113T + 3.5014$	kJ kg^{-1} K^{-1}	37
$Cp_f(T)$	Frozen matrix [a] specific heat [c d]	$0.0068T + 0.0907$	kJ kg^{-1} K^{-1}	17,20

[a] 15% (w/w) sucrose

[b] valid in the range [267; 293] K

[c] valid in the range [223; 273] K

[d] where T is in [K]

Further analysis was done for subsequent nucleation, ice crystal growth phase, and cooling of the frozen product during CN1. It results that exchanged heat includes both latent and sensible heat as follows:

$$Q = m_s \Delta H_c + \int_{T_n}^{T_f} m_f Cp_f(T) dT \quad (3)$$

As shown in literature,[17–19] the mass density of the solution and of the frozen matrix was almost steady within the temperature range investigated and results from the combination of the mass density of water and sucrose:

$$\rho = \left(\sum_j \frac{x_j}{\rho_j} \right)^{-1} \quad (4)$$

Temperature variation of the specific heat capacity of the frozen product was described based on literature data.[17,20] Again, the heat calculated in Eq. (3) was compared with the experimental value obtained from time integration of the heat flux given by the AccuFlux sensor after multiplying it by the sensor area. A code was implemented in Matlab R2020b (The Mathworks Inc., Natick, MA, USA) to make such an assessment.

This analysis was repeated in the case of mid load conditions considering the primary drying phase (PD1). In the calculations, we assumed that all water in the vial was present as ice and, thus, removed via sublimation. Again, we focused this analysis on the central AccuFlux sensor.

2.3.4 In-line monitoring of freezing and primary drying

The ability of a heat flux sensor to capture the main thermal events during the freezing phase was tested during spontaneous and controlled nucleation. These trials were named MSN1 and MCN1 (see details in Table 1).

Furthermore, heat flux sensors were used for the monitoring of primary drying in the case of controlled and spontaneous nucleation, respectively (see MPD1 and MPD2 in Table 1). While using ice-fog-controlled nucleation (MPD1), an injected water volume of 40 mL was chosen to avoid bad distribution of ice-fog across the batch, since larger trays were used. An additional analysis was carried out to test the sensor's ability to detect the end of primary drying, exploiting both MPD1 and MPD2 runs, as proposed by Fissore et al.,[21] and validated by Vollrath et al.,.[22]

3 RESULTS

3.1 Validation of the heat flux sensor's signal

The performance of the heat flux sensors was first tested for their ability to detect the heat flux exchanged between the shelf and the vials during the cooling of the liquid (test CN1 in Table 1). Figure 3 shows a positive agreement between the theoretical heat flux profile, as calculated by Eq. (2), and AccuFlux signals. Because of the noise in the thermocouple signals, the theoretical heat flux profile was smoothed in Matlab by applying the Savitzky-Golay filter. The normalized root-mean-square error (NRMSE) was calculated to compare the experimental values (black solid curve in Figure 3) and the theoretical values (blue dotted curve in Figure 3). Using the data range as a means of normalization, we found an NRMSE equal to 5%, which highlights the accuracy of the AccuFlux heat flux measurement.

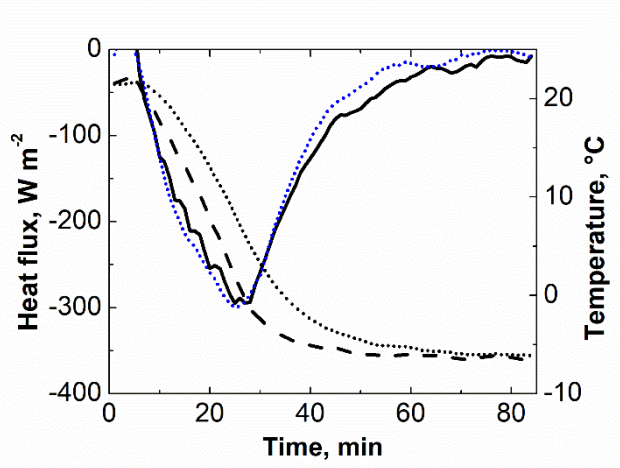

Figure 3. Comparison between the evolution of heat flux during freezing as detected by the AccuFlux sensor (black solid curve) and theoretically calculated (blue dotted curve). Product and sensor temperatures are also represented as black dotted and dashed curves respectively. Refers to run CN1.

Afterwards, we tested the ability of heat flux sensors to track the nucleation event and subsequent ice crystal growth. According to Eq. (3), the theoretical sensible and latent heat exchanged during run CN1 was

-4.87×10^3 J, which is aligned with the value obtained by time integration of the heat flow rate signal, as measured by the AccuFlux sensor, i.e., -4.88×10^3 J. This test was duplicated and confirmed the consistency between AccuFlux signal and theoretical calculations.

Additionally, we tested the ability of the central AccuFlux to estimate the amount of heat supplied by the temperature-controlled shelf to the vial during primary drying (test PD1 in Table 1). Unfortunately, the heat flux sensor seemed to underestimate the amount of heat exchanged during primary drying. In fact, the theoretical value of heat necessary to complete the sublimation of ice in the monitored vials was 35.1×10^3 J, while the value estimated by time integration of the AccuFlux sensor was 5.6×10^3 J. This discrepancy could be due to the fact that the monitored vials did not receive heat only by the temperature-controlled shelf, but also by radiation and gas conduction from the environment of the drying chamber.[9,10] However, this hypothesis has not been validated yet and further investigation is needed. A second run was carried out, confirming these results.

3.2 On the use of heat flux sensors for in-line monitoring of freezing

The AccuFlux sensors were used to monitor the heat flux between the temperature-controlled shelf and the vials during an uncontrolled freezing protocol (test MSN1 in Table 1). As mentioned in previous studies,[1,23] the nucleation event can be highlighted in the heat flux plot by downward spikes due to the release of heat; reasonably, multiple nucleation events are visible in the representation of MSN1 in Figure 4, each referring to individual vials. The use of heat flux sensors shows some clear advantages. Their primary strength lies in the capability to detect a nucleation event across the batch without causing any perturbation to the system, independently of the spontaneous or controlled onset of nucleation. In fact, if thermocouples are used, it is well-known that they can act as preferential sites for nucleation.[12,21] Secondly, the sensors allow the detection of the onset and offset of the nucleation events (shown in Figure 4) and consequently the range of nucleation temperatures at least for the monitored vials which are placed on top of the sensor. This information is of great significance because, as shown by others,[4,24–26] the morphology of the lyophilized products strongly depends on, and can also be predicted by, the range of their nucleation temperature.

Afterwards, a similar investigation was carried out in the case of control of nucleation temperature by the application of the ice-fog technique (test MCN1 in Table 1). For the sake of clarity, the observed potentials for the heat flux sensors are thereafter discussed in separate sections (3.2.1, 3.2.2 and 3.2.3).

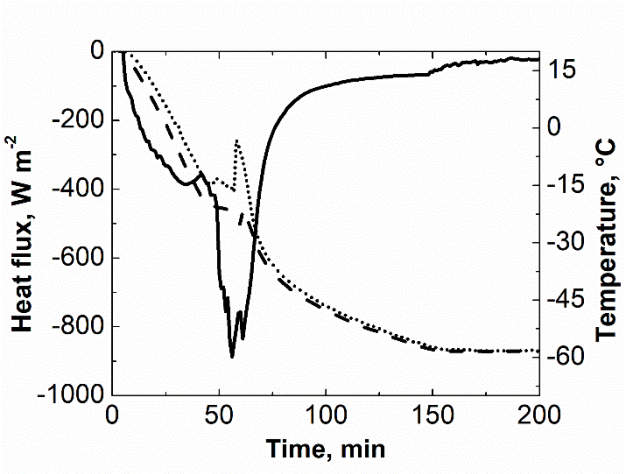

Figure 4. Evolution of heat flux as detected by the AccuFlux sensor (solid curve) in the case of spontaneous nucleation (refers to run MSN1). The dotted curve represents the temperature profile given by a thermocouple while the dashed curve represents the sensor temperature.

3.2.1 Vial conditioning

Conditioning the samples at the desired temperature is fundamental for an accurate control of their nucleation temperature. In this regard, the AccuFlux sensors can detect the time at which the temperature of all the monitored vials levelled off over a plateau value, indicating that steady-state conditions have been achieved. As shown in Figure 5 (points A-B), the AccuFlux heat flux initially increased because of sample cooling and, then, gradually levelled off over a constant value close to zero. This last trend indicated that the temperature of all the monitored vials was uniform and constant over time and, thus, ice crystals can be introduced into the drying chamber to trigger nucleation. This approach results in a precise control of the ‘conditioning time’ and avoids the operation to become longer than necessary. Furthermore, by using AccuFlux sensors, the user can detect any process deviation and take appropriate corrective actions by adjusting the conditioning time according to their heat flux trend.

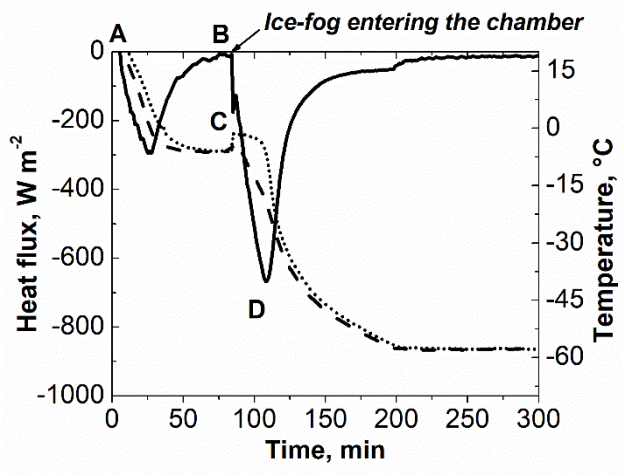

Figure 5. Evolution of heat flux as detected by the AccuFlux sensor (solid curve) in the case of controlled nucleation (refers to run MCN1). The dotted curve represents the temperature profile given by a thermocouple while the dashed curve represents the sensor temperature.

3.2.2 Control of nucleation temperature

We also tested the AccuFlux sensors in the case of controlled freezing (test MCN1 in Table 1). Once the ice-fog entered the freeze-drying chamber, a unique nucleation event occurred across the batch and a single downward spike in the AccuFlux heat flux profile was visible and is shown in Figure 5 (points B-C).

In contrast, the AccuFlux signal showed multiple peaks in the case of uncontrolled freezing (test MSN1 in Table 1), as shown in Figure 4 and previously discussed in Section 3.2. It follows that the AccuFlux sensors can effectively detect the nucleation of individual vials without being invasive.

Inversely, Figure 6 shows the AccuFlux outcomes when ice-fog prematurely entered the freeze-drying chamber (test CN2 in Table 1), i.e., before all vials were equilibrated to the same temperature. Another proof is provided by the thermocouple signal, of which the vial showed nucleation almost forty minutes after ice-fog was introduced. It must be said that we could not state the exact number of vials per sensor that nucleated later only on the basis of the detected heat profile. In fact, the instant heat release depends on multiple and hard-to-correlate conditions. Furthermore, we investigated the thermal history of vials placed on and off the edge sensor of the second shelf to assess the invasiveness of the device in a freezing test. As shown in Figure 7, all the monitored vials showed similar cooling behaviour, which supports the theory that the sensor does not alter the heat transfer efficiency between shelf and vials. The nucleation event is not shown in Figure 7 because the vials monitored by thermocouples are not representative of the batch as a whole. Nevertheless, we used a video camera to track the nucleation time of the other vials placed off the sensor and not equipped with a

thermocouple. As shown in Figure 8, all monitored vials nucleated within 10 s once nucleation was triggered for the batch.

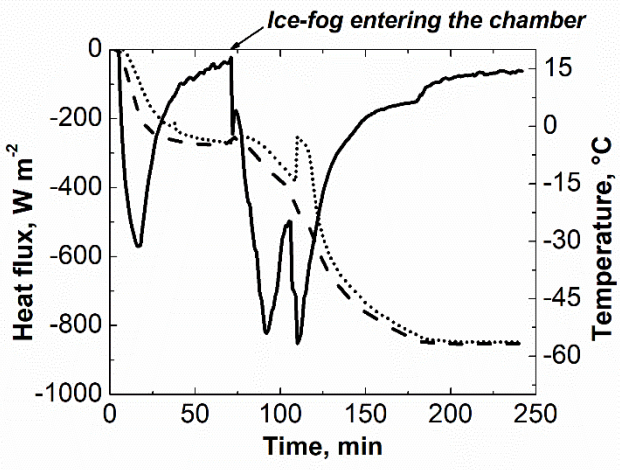

Figure 6. Evolution of heat flux as detected by the AccuFlux sensor (solid curve) when nucleation was prematurely triggered (refers to run CN2). The dotted curve represents the temperature profile given by a thermocouple while the dashed curve represents the sensor temperature.

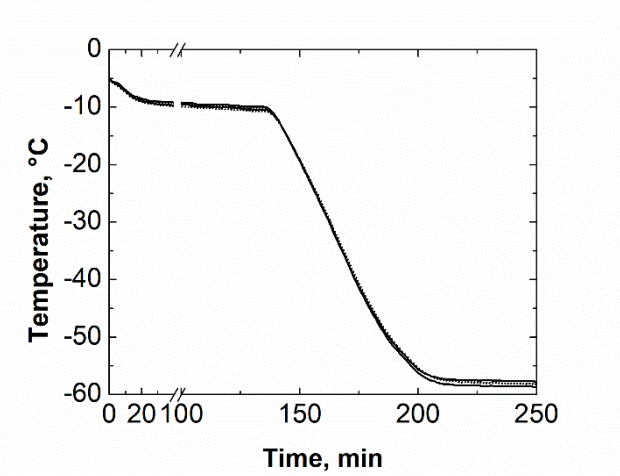

Figure 7. Temperature evolution detected by thermocouples placed on the sensor (solid curves) and off the sensor (dotted curves). The nucleation event is not represented because thermocouples introduce a bias in monitored vials compared to non-monitored vials.

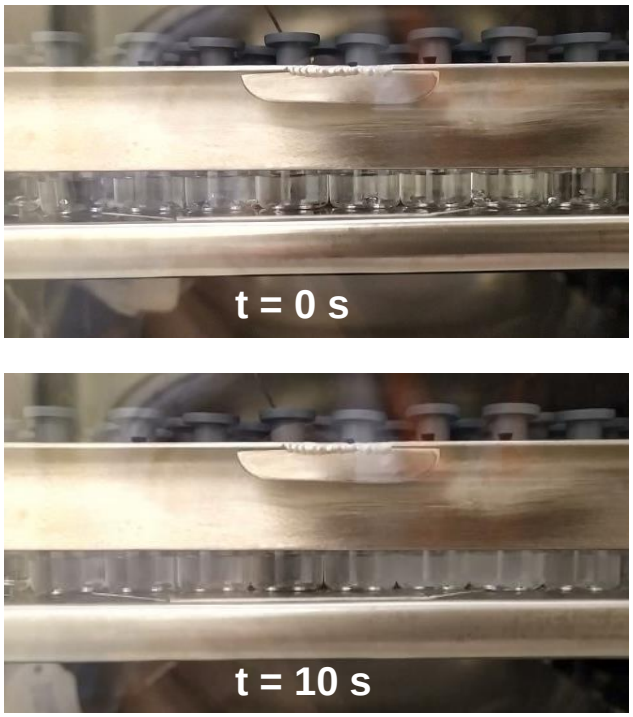

Figure 8. Nucleation event for vials placed off the sensor within a time span of 10 s.

3.2.3 Ice crystal growth and freezing rate

During the ice crystal growth phase (see points C-D in Figure 5), product temperature did not change once the vials were nucleated, whereas the heat flux did. During this step, the rate at which heat is removed from the vials, known as the freezing rate, has a direct impact on the final ice structure.[23,27] The depth of heat flux profile represented an effective way to monitor freezing rate and subsequent crystal growth. For example, the freezing rate for the MCN1 test was – 1 °C/min and resulted in a certain heat flux evolution (as visible in Figure 5). If faster freezing had been chosen, we would have expected deeper V-profiles and therefore smaller ice crystals would have been produced.

Furthermore, we could recognize the termination of crystal growth in point D in Figure 5, where the exchange of latent heat ended; from that point forward the samples went through solidification. An additional usefulness of the device lies in the ability to detect the completion of solidification. When the solutions were completely frozen no more heat had to be removed from the samples and the heat flux approached zero. This feature turned out to be essential to reduce processing time during freezing.

Finally, we investigated the invasiveness of the AccuFlux sensor on crystal growth. To this end, we analyzed the temperature evolution detected by thermocouples placed on and off the sensor and observed similar behavior of the monitored vials during crystal growth, as shown in Figure 7.

3.3 Experimental validation of heat flux sensors for in-line monitoring of primary drying

The ability of AccuFlux sensors to detect the primary drying endpoint was evaluated[21,22] (cycles MPD1 and MPD2 in Table 1). Figure 9 shows the evolution of heat flux in MPD1 for vials placed in the centre and on the edge of the second temperature-controlled shelf. The vials were heated through the sublimation step and, consequently, heat evolution is shown on the positive y-axis. When heat flux stabilized at a value around zero, primary drying for the monitored vials could be considered satisfactorily completed. As expected, ice sublimation for vials placed on the edge was complete before the vials located in the centre. This result agrees with the product temperature evolutions shown in Figure 9; as reported by various authors,[13,14] actually, ice sublimation completion can be recognized by the sharp increase in product temperature since ice sublimation does not use any of the heat transferred from equipment to products. Moreover, vials located at different locations on the shelf are expected to show heterogeneity in terms of heat transfer coefficient because of the different heat transfer mechanism involved.[8,28] In this respect, the K_v of edge vials will be higher than that of vials placed in the core of the batch.

Another remarkable difference between the two heat flux profiles lies within the onset-offset of the heat flux drop, which is used as an indicator of the with-in batch heterogeneity; the larger it is, the more the sublimation behaviour of the vials within the batch is different. Accordingly, the onset-offset time for the central vials is shorter than for the vials on the edge, due to their greater uniformity. A significant observation can be highlighted with respect to the pressure profiles reported in Figure 9. The majority of the vials within the batch act like central vials rather than edge and thus, the Pirani pressure signal starts decreasing only when the central vials are done with the sublimation step. Finally, it must be noted that the onset-offset time of the heat flux drop for a given sensor (edge of the second shelf) is shorter (seven to eight hours) with respect to an uncontrolled nucleation freeze-drying protocol (MPD2). As widely reported,[1,2] in fact, controlled nucleation technologies aim at eliminating vials' heterogeneity in freezing which, in turn, has a direct impact on their drying behaviour.

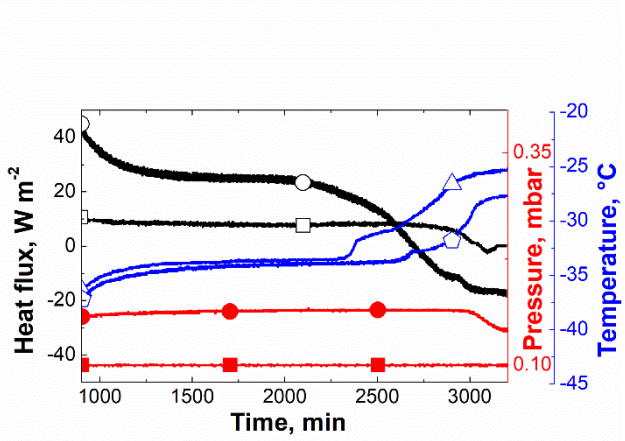

Figure 9. Evolution of heat fluxes, temperatures and pressures recorded during primary drying (refers to run MPD1). Heat fluxes detected by the AccuFlux sensors for central and edge vials are represented by the black curves (□ and ○ respectively). The temperature profiles for central and edge vials are represented by the blue curves (⬠ and △ respectively). Pressure signals are also shown through the red curves, i.e., capacitance manometer's (■) and Pirani's (●).

3.4 Design space for freezing and primary drying through heat flux sensors

In light of the positive features outlined, the AccuFlux sensors can support professionals in cycle transfer or scale-up from different pieces of equipment. It is well-known that a freeze-drying cycle developed on the laboratory scale may fail if applied to a large-scale unit as such and, thus, its design space is broadly investigated for both quality and economic perspectives.[29–32] For establishing the design space, a well-defined number of experiments is needed to obtain the required parameters to describe and then predict the cycle. Several techniques have been developed to assess these parameters, but they can be slow, invasive and not applicable to any freeze-dryer. To provide an example, we created a design space for primary drying for edge vials in the context of MPD1 and MPD2 cycles (Figures 10(a), 10(b), 11(a), 11(b)), where the freezing steps were run with controlled and spontaneous nucleation, respectively. We followed a similar methodology to that reported by Carfagna et al.;[33] we estimated the heat transfer coefficient and, thus, the product resistance from the heat flux recorded by the edge sensor of the second shelf. In particular, given a 4 mm thickness of the dried layer, we found that in the controlled nucleation run, K_v was higher compared to the spontaneous nucleation run (17.3 W m^{-2} K^{-1} in MPD1, 19.5 W m^{-2} K^{-1} in MPD2) while the product resistance, R_p, was lower (4.43×10^5 Pa m^2 s kg^{-1} in MPD1, 3.55×10^5 Pa m^2 s kg^{-1} in MPD2).

The curves shown in Figures 10(a) and 10(b) identify the highest value of shelf temperature that preserves product quality for the considered values of L_{dried}/L and chamber pressure. As the primary drying goes on, i.e., increasing the value of L_{dried}/L, the design space gradually shrinks due to the increment of R_p in respect to L_{dried}. Given a value of L_{dried}/L, higher shelf temperature and lower chamber pressure could be selected in MPD1 with respect to MPD2 to ensure product quality, as shown in Figures 10(a) and 10(b) respectively. For a conservative design space, the ideal recipe can be obtained using the curve at L_{dried}/L = 99%, at which point the parameters specified in the curve provide operating conditions that ensure product quality throughout the entire primary drying and are bounded by the shaded areas in Figures 11(a) and 11(b). To minimize cycle time, processing conditions should be selected as close as possible to the highest sublimation rate, as indicated in the blue shaded areas in Figure 11. As a result, when the controlled nucleation protocol was used (MPD1), a higher shelf temperature and lower chamber pressure than those used during the spontaneous nucleation test (MPD2) could be chosen to maximise the sublimation rate.

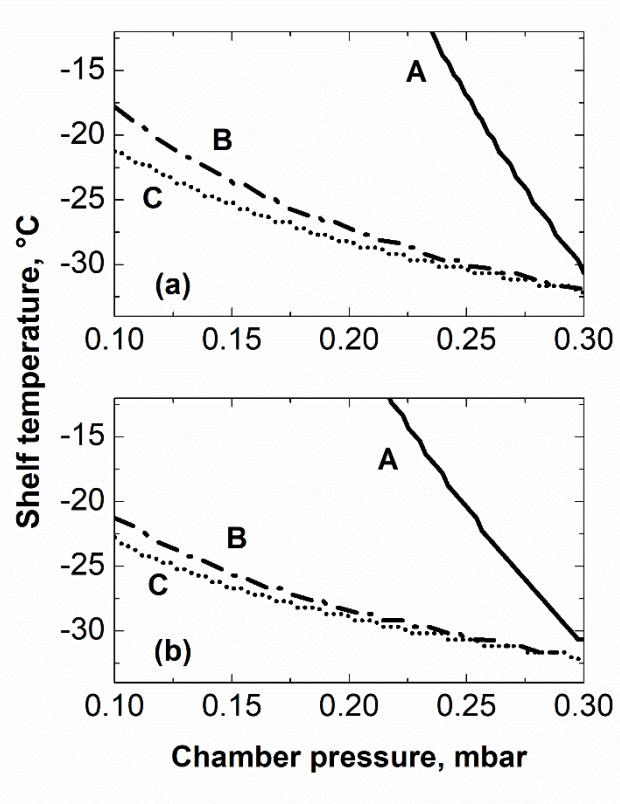

Figure 10. Design space calculated at different values of L_{dried}/L for MPD1 (Figure 10(a)) and MPD2 (Figure 10(b)): 1% (A), 30% (B) and 99% (C). The area under each curve provides the combination of shelf temperature and chamber pressure specified by the L_{dried}/L ratio.

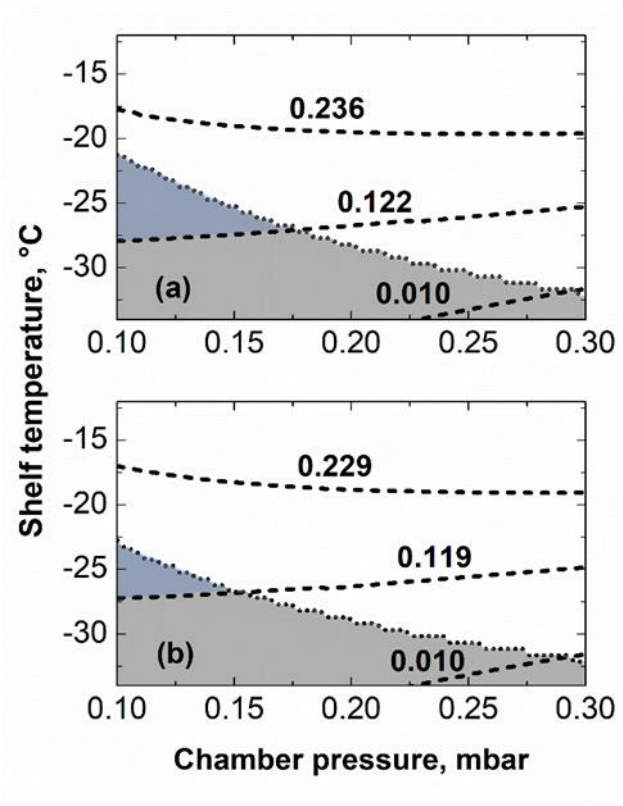

Figure 11. Design space calculated at L_{dried}/L = 99% for MPD1 (Figure 11(a)) and MPD2 (Figure 11(b)). The dotted curves identify the operating condition limits. The dashed curves give the combination of shelf temperature and chamber pressure that produce the indicated value of J_w (in kg h^{-1} m^{-2}) near the endpoint of drying. The shaded areas display the set of processing conditions that ensure product quality. The blue shaded areas indicate the areas of the design space with the highest sublimation rate.

Furthermore, our study provides considerable insight about the freezing step; we believe that a design space for freezing could also be designed by exploiting the sensors. Undertaking an approach similar to that of Arsiccio and Pisano,[29] heat flux sensors might be used to determine the freezing front velocity and, hence, help to build a design space for freezing.

4 CONCLUSIONS

In the present work, heat flux sensors were exploited to analyse heat flux evolution over freeze-drying cycles for a sucrose-based formulation. Beforehand, validation tests were carried out to verify measured data. Afterwards, the in-line monitoring of freezing and primary drying by means of heat flux sensors was investigated. The results clearly show the potential of the devices, which allow an easier and more robust control of the lyophilization process and provide a better understanding of the physical phenomena involved.

For proper implementation, multiple sensors should be mounted in different locations on the temperature-controlled shelves; this is of great significance as the size of the freeze-dryer increases, increasing the heterogeneity of the temperature gradient over the shelf and between shelves.

Finally, heat flux sensors could be used as a practical tool for building the design space for freezing and primary drying.

Author contributions

Camilla Moino, Erwan Bourlès, Roberto Pisano and Bernadette Scutellà were involved in the conception and design of the study. Camilla Moino acquired the data, analysed and interpreted the experimental results. All authors were involved in drafting the manuscript or revising it critically for important intellectual content. All authors had full access to the data and approved the manuscript before it was submitted by the corresponding author.

Acknowledgements

The authors would like to thank Vincent Ronsse (GSK Vaccines technician) and Alain Philippart (GSK Vaccines operator) for their valuable help during sample preparation and experimental set-ups.

Funding

This work was sponsored and financially supported by GlaxoSmithKline Biologicals SA.

Conflict of Interest

Erwan Bourlès and Bernadette Scutellà are employees of the GSK group of companies. Camilla Moino was holding a Master Thesis studentship and collaborated with GSK at the time of the study as part of her Master Thesis training. The other authors have no conflict of interest to declare.

NOMENCLATURE

a sensor length, m

b sensor width, m

Cp_f specific heat capacity of a 15% (w/w) sucrose frozen matrix, kJ kg^{-1} K^{-1}

Cp_s specific heat capacity of a 15% (w/w) sucrose solution, kJ kg^{-1} K^{-1}

J_w sublimation flux, kg h^{-1} m^{-2}

J_q heat flux, W m^{-2}

K_v heat transfer coefficient, W m^{-2} K^{-1}

L total product thickness, m

L_{dried} thickness of the dried layer, m

m_f mass of a 15% (w/w) sucrose frozen matrix, kg

m_s mass of a 15% (w/w) sucrose solution, kg

N_v maximum number of vials per sensor, -

Q heat, J

$\dot{Q}_c$ heat flow rate in cooling, W

r vial radius, m

R_p product resistance, Pa m^2 s kg^{-1}

t time, min

T temperature, °C

T_f final freezing temperature, °C

T_n nucleation temperature, °C

x percentage by weight, -

ΔH_c enthalpy of crystallization of a 15% (w/w) sucrose solution, kJ kg^{-1}

ΔH_s enthalpy of sublimation of water, kJ kg^{-1}

Δt time step, s

GREEK LETTERS

ρ mass density, kg dm^{-3}

ρ_f mass density of a 15% (w/w) sucrose frozen matrix, kg dm^{-3}

ρ_s mass density of a 15% (w/w) sucrose solution, kg dm^{-3}

SUBSCRIPTS

i time index, -

j component index, -

REFERENCES

(1) Assegehegn, G.; Brito-de la Fuente, E.; Franco, J. M.; Gallegos, C. The Importance of Understanding the Freezing Step and Its Impact on Freeze-Drying Process Performance. *J. Pharm. Sci.* **2019**, *108* (4), 1378–1395.

(2) Pisano, R. Alternative Methods of Controlling Nucleation in Freeze Drying. In L*yophilization of Pharmaceuticals and Biologicals: New Technologies and Approaches*; Ward, K. R., Matejtschuk, P., Eds.; **2019**; pp 79–11.

(3) Bursac, R.; Sever, R.; Hunek, B. A Practical Method for Resolving the Nucleation Problem in Lyophilization. *Bioprocess Int.* **2009**, *7* (9), 66–72.

(4) Searles, J. A.; Carpenter, J. F.; Randolph, T. W. The Ice Nucleation Temperature Determines the Primary Drying Rate of Lyophilization for Samples Frozen on a Temperature-Controlled Shelf. *J. Pharm. Sci.* **2001**, *90* (7), 860–871.

(5) Hottot, A.; Vessot, S.; Andrieu, J. Freeze Drying of Pharmaceuticals in Vials: Influence of Freezing Protocol and Sample Configuration on Ice Morphology and Freeze-Dried Cake Texture. *Chem. Eng. Process. Process Intensif.* **2007**, *46* (7), 666–674.

(6) Pisano, R.; Arsiccio, A.; Nakagawa, K.; Barresi, A. A. Tuning, Measurement and Prediction of the Impact of Freezing on Product Morphology: A Step toward Improved Design of Freeze-Drying Cycles. *Dry. Technol.* **2019**, *37* (5), 579–599.

(7) Chakravarty, P.; Lee, R.; Demarco, F.; Renzi, E. Ice Fog as a Means to Induce Uniform Ice Nucleation during Lyophilization. *BioPharm International*. **2012**, pp 33–38.

(8) Rambhatla, S.; Pikal, M. J. Heat and Mass Transfer Scale-up Issues during Freeze-Drying, I: Atypical Radiation and the Edge Vial Effect. *AAPS PharmSciTech* **2003**, *4* (2), 1–10.

(9) Scutellà, B.; Passot, S.; Bourlés, E.; Fonseca, F.; Tréléa, I. C. How Vial Geometry Variability Influences Heat Transfer and Product Temperature During Freeze-Drying. *J. Pharm. Sci.* **2017**, *106* (3), 770–778.

(10) Scutellà, B.; Trelea, I. C.; Bourlès, E.; Fonseca, F.; Passot, S. Determination of the Dried Product Resistance Variability and Its Influence on the Product Temperature in Pharmaceutical Freeze-Drying. *Eur. J. Pharm. Biopharm.* **2018**, *128*, 379–388.

(11) Nail, S. L.; Johnson, W. Methodology for In-Process Determination of Residual Water in Freeze-Dried

Products. *Developments in biological standardization*. **1992**.

(12) Nail, S.; Tchessalov, S.; Shalaev, E.; Ganguly, A.; Renzi, E.; Dimarco, F.; Wegiel, L.; Ferris, S.; Kessler, W.; Pikal, M.; Sacha, G.; Alexeenko, A.; Thompson, T. N.; Reiter, C.; Searles, J.; Coiteux, P. Recommended Best Practices for Process Monitoring Instrumentation in Pharmaceutical Freeze Drying—2017. *AAPS PharmSciTech* **2017**, *18* (7), 2379–2393.

(13) Patel, S. M.; Doen, T.; Pikal, M. J. Determination of End Point of Primary Drying in Freeze-Drying Process Control. *AAPS PharmSciTech* **2010**, *11* (1), 73–84.

(14) Pisano, R. Automatic Control of a Freeze-Drying Process: Detection of the End Point of Primary Drying. *Dry. Technol.* **2020**, 1–18.

(15) Ganguly, A.; Stewart, J.; Rhoden, A.; Volny, M.; Saad, N. Mass Spectrometry in Freeze-Drying: Motivations for Using a Bespoke PAT for Laboratory and Production Environment. *Eur. J. Pharm. Biopharm.* **2018**, *127* (March), 298–308.

(16) Meyer, V. M.; Keller, B. A New Heat Flux Sensor: From Microvolts to Millivolts. *Sensors Mater.* **1996**, *8* (6), 345–356.

(17) Feistel, R.; Wagner, W. A New Equation of State for H2O Ice Ih. *J. Phys. Chem. Ref. Data* **2006**, *35* (2), 1021–1047.

(18) Rowe, R. C.; Sheskey, P. J.; Quinn, M. E. *Handbook of Pharmaceutical Excipients*, 6th ed.; USA, **2009**.

(19) Perry, R. H.; Green, D. W.; Maloney, J. O. *Perry's Chemical Engineers' Handbook*; **2000**; Vol. 38.

(20) Putnam, R. L.; Boerio-Goates, J. Heat-Capacity Measurements and Thermodynamic Functions of Crystalline Sucrose at Temperatures from 5 K to 342 K. Revised Values for ΔfGom(Sucrose, Cr, 298.15 K), ΔfGom(Sucrose, Aq, 298.15 K), Som(Sucrose, Aq, 298.15 K); and ΔrGom(298.15 K) for the Hydroly. *The Journal of Chemical Thermodynamics*. **1993**, pp 607–613.

(21) Fissore, D.; Pisano, R.; Barresi, A. A. Process Analytical Technology for Monitoring Pharmaceuticals Freeze-Drying–A Comprehensive Review. *Dry. Technol.* **2018**, *36* (15), 1839–1865.

(22) Vollrath, I.; Pauli, V.; Friess, W.; Freitag, A.; Hawe, A.; Winter, G. Evaluation of Heat Flux Measurement as a New Process Analytical Technology Monitoring Tool in Freeze Drying. *J. Pharm. Sci.* **2017**, *106* (5), 1249–1257.

(23) Thompson, T. N. LyoPAT™: Real-Time Monitoring and Control of the Freezing and Primary Drying Stages during Freeze-Drying for Improved Product Quality and Reduced Cycle Times. *American Pharmaceutical Review*. **2013**.

(24) Arsiccio, A.; Barresi, A. A.; Pisano, R. Prediction of Ice Crystal Size Distribution after Freezing of Pharmaceutical Solutions. *Cryst. Growth Des.* **2017**, *17* (9), 4573–4581.

(25) Arsiccio, A.; Barresi, A.; De Beer, T.; Oddone, I.; Van Bockstal, P. J.; Pisano, R. Vacuum Induced Surface Freezing as an Effective Method for Improved Inter- and Intra-Vial Product Homogeneity. *Eur. J. Pharm. Biopharm.* **2018**, *128*, 210–219.

(26) Capozzi, L. C.; Pisano, R. Looking inside the 'Black Box': Freezing Engineering to Ensure the Quality of Freeze-Dried Biopharmaceuticals. *Eur. J. Pharm. Biopharm.* **2018**, *129*, 58–65.

(27) Searles, J. A. Freezing and Annealing Phenomena in Lyophilization. In *Freeze-Drying/Lyophilization of Pharmaceutical and Biological Products*; Dekker, M., Ed.; New York, **2004**; pp 109–145.

(28) Pisano, R.; Fissore, D.; Barresi, A. A. Heat Transfer in Freeze-Drying Apparatus. In *Developments in Heat Transfer*; InTech, Ed.; Rijeka, Croatia, **2011**; pp 91–114**.**

(29) Arsiccio, A.; Pisano, R. Application of the Quality by Design Approach to the Freezing Step of Freeze-Drying: Building the Design Space. *J. Pharm. Sci.* **2018**, *107* (6), 1586–1596.

(30) Arsiccio, A.; Giorsello, P.; Marenco, L.; Pisano, R. Considerations on Protein Stability During Freezing and Its Impact on the Freeze-Drying Cycle: A Design Space Approach. *J. Pharm. Sci.* **2020**, *109* (1), 464–475.

(31) Fissore, D.; Pisano, R.; Barresi, A. A. Advanced Approach to Build the Design Space for the Primary Drying of a Pharmaceutical Freeze-Drying Process. *J. Pharm. Sci.* **2011**, *100*, 4922–4933.

(32) Kawasaki, H.; Shimanouchi, T.; Takahashi, K.; Kimura, Y. Effect of Controlled Nucleation of Ice Crystals on the Primary Drying Stage during Lyophilization. *Chem. Pharm. Bull.* **2018**, *66* (12), 1122–1130.

(33) Carfagna, M.; Rosa, M.; Lucke, M.; Hawe, A.; Frieß, W. Heat Flux Sensor to Create a Design Space for Freeze-Drying Development. *Eur. J. Pharm. Biopharm.* **2020**, *153*, 84–94.

(34) Pisano, R.; Fissore, D.; Barresi, A. A.; Brayard, P.; Chouvenc, P.; Woinet, B. Quality by Design: Optimization of a Freeze-Drying Cycle via Design Space in Case of Heterogeneous Drying Behavior and Influence of the Freezing Protocol. *Pharm. Dev. Technol.* **2013**, *18* (1), 280–295.

(35) Wang, G. M.; Haymet, A. D. J. Trehalose and Other Sugar Solutions at Low Temperature: Modulated Differential Scanning Calorimetry (MDSC). *J. Phys. Chem. B* **1998**, *102* (27), 5341–5347.

(36) Feistel, R.; Wagner, W. Sublimation Pressure and Sublimation Enthalpy of H2O Ice Ih between 0 and 273.16 K. *Geochim. Cosmochim. Acta* **2007**, *71* (1), 36–45.

(37) Mohos, F. Á. Appendix 1: Data on Engineering Properties of Materials Used and Made by the

Confectionery Industry. In *Confectionery and Chocolate Engineering: Principles and Application*; **2016**; pp 617–642.

For Table of Contents only: